Research Square

Preprints are preliminary reports that have not undergone peer review.
They should not be considered conclusive, used to inform clinical practice,
or referenced by the media as validated information.

Surface free electrons endow 2D Alkali metal nitrides with extraordinary adsorption on volatile organic compounds

Jintian Wang
Chongqing University
Shu Li
Army Medical University (Third Military Medical University)
Xuan Zhang
Army Medical University (Third Military Medical University)
Qian Chen
hetoqc@tmmu.edu.cn

Army Medical University (Third Military Medical University)
Miao Zhou
Chongqing University

Article

Keywords: volatile organic compounds (VOCs), 2D Alkali metal nitrides, Ca2N, Sr2N, Ba2N, First principles calculations, 2D electronic compounds

Posted Date: March 3rd, 2026

DOI: https://doi.org/10.21203/rs.3.rs-8852905/v1

License: This work is licensed under a Creative Commons Attribution 4.0 International License.
Read Full License

Additional Declarations: No competing interests reported.

Abstract

Volatile organic compounds (VOCs) are a major cause of leukemia, carcinoma, and other diseases. However, removal technologies for VOCs cannot cope with the grim situation of VOC pollution. Two-dimensional (2D) alkali metal nitrides Ca_2N, Sr_2N, and Ba_2N have great potential as a new adsorption material, and their application as a VOCs detector has not reported. Here, we study the sensing performance of Ca_2N, Sr_2N, and Ba_2N on benzene, styrene, xylene, methylbenzene, ethylbenzene, butyl acetate, methanal, and n-undecane. We find that Ca_2N, Sr_2N, and Ba_2N have outstanding adsorption capabilities for VOCs. This strong adsorption is attributed to the free-electron layer on their surface. When the isosurfaces are equal, there are more free electrons on the surface of Ca2N, followed by Sr2N, and finally Ba2N. Moreover, electric fields could effectively improve their adsorption performance. The perfect match of the electronic properties of VOCs with those of Ca2N, Sr2N, and Ba2N contributes to this extraordinary adsorption capability. Therefore, this study will lead to a new round of technological innovation in VOCs adsorption technology based on 2D alkali metal nitrides.

Introduction

Volatile organic compounds (VOCs) such as benzene, formaldehyde, and toluene usually accumulate indoors[1]. In national environmental health surveys conducted in the United States, Canada, and South Korea, over 90% participants had detected metabolites of benzene in their urine[2–4]. Long term exposure to high concentrations of VOCs causes various hazards to the human body. Skin and eye contact with methanal cause dryness and ulcers[5]. Long-term exposure to VOCs will not only damage the human respiratory[6], hematopoietic, immune, digestive and reproductive systems[7], but also lead to pneumonia, chronic obstructive pulmonary disease[8], leukemia, lymphoma, bladder cancer and other diseases[9]. VOCs also increase the risk of depression and other mental diseases[10,11]. Besides, a negative correlation between VOCs exposure and adolescent growth indicators was found[12]. Moreover, elevated levels of VOCs in urine were significantly and positively correlated with an increase in the plasma atherogenic index[13]. The urinary metabolites of ethylbenzene and styrene were significantly associated with cardiovascular disease, respiratory disease, and cancer mortality[14]. In addition, the normal and pathological states of human physiological processes can be characterized by the VOCs released during respiration[15–17]. Therefore, the detection and removal of these pollutants is of great significance.

Numerous VOC control technologies have emerged, such as incineration, condensation, biological degradation, absorption, adsorption, and catalytic oxidation, et al[18,19]. Among them, the adsorption technology has been recognized as an efficient and economical control strategy[20–22]. In current research on VOCs adsorption, traditional light absorption sensors[23], heat conduction sensors[24] have insufficient adsorption capacity[24]. Carbon materials suffer from poor renewability, fire risks, high mass transfer resistance, pore blockage, and hygroscopicity[25,26]. Zeolites and metal organic frameworks materials are costly, with numerous voids leading to weak dispersion forces and insufficient open metal sites[27,28].

Organic polymers involve complex synthesis processes, making large-scale production challenging[29]. Adsorption and membrane separation processes have poor adsorption capacity and selectivity for VOCs[30]. The average specific surface area, pore volume and VOCs adsorption capacity of different adsorption materials are metal organic frameworks > activated carbons > hypercrosslinked polymeric resin > zeolites[31,32]. However, the focus of these studies is on the specific surface area, adsorption pore size, and number of functional groups of the adsorbent, without considering the electronic interaction between the adsorbent and VOCs molecules[33,34]. Therefore, it is vital to explore the enormous potential of two-dimensional (2D) electronic materials in the field of gas adsorption by utilizing their unique structures and surface properties.

2D electronic compounds own the advantages of a large specific surface area, high mechanical strength, as well as the high electron concentration, high active site density[35,36], and low work function of electronic compounds[37–41]. Alkali metal nitrides Ca_2N, Sr_2N, and Ba_2N are classical 2D electronic compounds that can be separated into single-layer structures in the laboratory[42]. They present M_2N (M = Ca, Ba, Sr), in which conduction electrons are confined between the M layers[42]. The delocalized homogeneous electrons in the 2D interlayer space are responsible for the excellent transport characteristics, which are mainly conducted through the 2D space instead of the M_2N layer[41–43]. However, the application of 2D electronic compounds in the sensing and detection of VOCs molecules has not been reported yet. In this work, we selected Ca_2N, Sr_2N, and Ba_2N as substrate materials and benzene, styrene, xylene, methylbenzene, ethylbenzene, butyl acetate, methanal, and n-undecane as adsorption targets. Based on first principles study, the adsorption of VOCs on a single-layer 2D electronic compound substrate was calculate. The adsorption capacity was adjusted by applying an electric field. The surface free electron layer properties of Ca_2N, Sr_2N, and Ba_2N endow them with powerful VOCs sensing capability and provide new technology for indoor air quality detection.

Results and Discussion

Geometric and Electronic Structures of Ca2N, Sr2N, and Ba2N

To investigate the properties of single-layer 2D electronic compounds Ca_2N, Sr_2N, and Ba_2N, we present the geometric and electronic structure of a single-layer 2D electronic compound in Fig. 1. Figure 1a shows the top and side views of a single-layer 2D electronic compound, where X represents Ca, Sr, and Ba[42,44]. The lattice structure of X_2N electronic compounds is hexagonal, with optimized lattice constants of a = b=3.62 Å (Ca_2N), a = b=3.81 Å (Sr_2N), and a = b=3.98 Å (Ba_2N). Each unit cell is composed of 2 X atoms and 1 N atom. From a top-down view, each X atom bonds to three adjacent N atoms, and each N atom is bonded to six adjacent X atoms. From a side view, X atoms construct the outer layers, and N atoms are in the middle layer. Figure 1b shows the partial charge density (left) and band structure diagram (right) of Ca_2N. In order to investigate the distribution of active electrons on the material

surface, the Fermi level was selected and the partial charge density of Ca_2N was calculated from − 1 eV to 1 eV, as shown in the left figure. The yellow areas (left) denote the charge density corresponding to the yellow energy range in the band diagram (right). Most of the charges near the Fermi level are distributed on the surface of the material. The distribution of free electrons on the material surface is mainly located between adjacent Ca atoms. The purple circle in the band diagram represents the projected energy band of free electrons in the surface space region of Ca_2N. The energy of surface electrons of Ca_2N is in the range of -1.2 eV to 1.5 eV. Similarly, Fig. 1c & 1d show the partial charge densities (left) and band structure diagrams (right) of Sr_2N and Ba_2N. The energy of surface electrons of Sr_2N ranges from − 1.1 eV to 1.4 eV, and the energy of surface electrons of Ba_2N ranges from − 0.8 eV to 1.5 eV. Comparing Fig. 1b-d, the projection regions of their surface free electrons in the band are similar, all located in the band near the Fermi level. The distribution of free electrons between adjacent Ca atoms is relatively uniform, while the distribution of free electrons between adjacent Sr/Ba atoms tends to lean towards the Sr/Ba atom on one side. During molecular adsorption, the electron-rich regions attract more molecules and result in charge transfer and adsorption. When the isosurfaces are equal, there are more free electrons on the surface of Ca_2N, followed by Sr_2N, and finally Ba_2N. These differences in their surface electrons result in their potential for molecular adsorption applications[45]. Collectively, Ca_2N, Sr_2N, and Ba_2N all have a hexagonal lattice structure and surface free electron distribution characteristics near the Fermi level. The differences in these structures and electronic properties characterize their adsorption applications.

Geometric and electronic structures of eight types of VOCs molecules

To investigate the adsorption of VOCs molecules by single-layer 2D electronic compounds, we then explore the geometric and electronic structures. We use m-xylene as a representative to calculate the adsorption of xylene[46]. Figure 2 shows the molecular structure of eight types of VOCs, presented in a top view and a sideview. The molecular electrostatic potential of these eight molecules is shown in Fig. 3[47].The blue area represents high energy and is prone to losing electrons. The red area indicates low energy and easy access to electrons. Both the red and blue areas represent more active areas on the surface of the molecule. In Fig. 3a, there is a portion of red area on the surface of the benzene molecule, located on both sides of the six C atoms on the benzene ring structure. However, the color around the H atom is not obvious. This indicates that the most active position of the benzene is located inside the benzene ring and is easily accessible to electrons[48,49]. The red area on the surface of the styrene (Fig. 3b) can be mainly divided into two parts. One part is located on both sides of the benzene ring structure, and the other part is around the C = C bond. Similarly, the alkyl functional groups in xylene (Fig. 3c), methylbenzene (Fig. 3d), and ethylbenzene (Fig. 3e) are not active, and the most active part is the benzene ring structure, which is easy to obtain electrons. The region around the C = O bond in butyl acetate (Fig. 3f) is the most active. In methanal (Fig. 3g), both the O atom side and the H atom side are relatively active, with the O atom side easily gaining electrons and the H atom side easily losing

electrons. The area around the H atom in n-undecane (Fig. 3h) is the most active and easily loses electrons, which differs from other VOCs. Taken together, these active regions provide a theoretical basis for subsequent research on adsorption interactions.

Adsorption of VOCs on Ca2N, Sr2N, and Ba2N Surface

We then calculate the adsorption of molecules at different angles and sites and select the structure with the lowest energy as the most stable structure. Table 1 presents the quantitative results of the equilibrium distance and adsorption energy of VOCs molecules. We find that methanol and butyl acetate have the shortest equilibrium distance, followed by styrene, xylene, methylbenzene, and ethylbenzene. Benzene has a longer distance and a significant decrease compared to the initial distance. N-undecane has no significant change in equilibrium distance compared to the initial distance. Besides, methanol and styrene have the highest adsorption energy, followed by xylene, methylbenzene, ethylbenzene, and butyl acetate. However, benzene and n-undecane have the lowest adsorption energy. These data indicate that Ca_2N substrates have the strongest adsorption effect on molecules containing C = O bonds. Molecules containing C = C, such as styrene, come next. Their adsorption energy is relatively high. Although benzene molecules have a benzene ring structure, the equilibrium distance does not change much from the initial distance. The n-undecane molecule shows no significant adsorption in terms of geometric structure, equilibrium distance, and adsorption energy. The H atoms on the surface of the molecule are prone to losing electrons, making it difficult to generate charge transfer with the free electrons on the Ca_2N substrate surface. These data demonstrate that the Ca_2N substrate exhibits the strongest adsorption of C = O bond-containing molecules and the weakest adsorption of n-undecane.

Figure 4 shows a side view of the combined structure of eight VOCs molecules and three electronic compound substrates after structural relaxation. On the Ca_2N substrate, benzene (Fig. 4a), styrene (Fig. 4b), xylene (Fig. 4c), methylbenzene (Fig. 4d), and ethylbenzene (Fig. 4e) are adsorbed at a horizontal angle. The position of the C = C bond in the styrene molecule is closest to the substrate, followed by the benzene ring structure inside the molecule. These indicate that the C = C bond structure is mainly adsorbed. Among the other four molecules, however, the benzene ring structure is closest to the substrate, while the alkyl structure in the molecule is farther away. Hence, the benzene ring structure is mainly adsorbed. Butyl acetate (Fig. 4f) is adsorbed at an inclined angle, with the O atoms that form the C = O bond closest to the substrate. The length of the C = O bond has been extended from the initial 1.22 Å to 1.44 Å, and some atoms are further away from the substrate than their initial position. This indicates that the substrate has a stronger adsorption effect on the O atom in the C = O bond and a weaker adsorption effect on the remaining atoms. The O atom in the methanal (Fig. 4g) is closest to the substrate, and the C = O bond is no longer in the same plane as the C and H atoms, implying that the O atom is strongly adsorbed by the substrate, while the H atom is subjected to a repulsive force towards the outside of the substrate. The n-undecane molecule did not undergo any deformation or change in position during the reaction.

The adsorption results of these VOCs molecules on Sr_2N (Fig. 4i-p) and Ba_2N (Fig. 4m-t) substrates are basically consistent with those on Ca_2N substrates. All three substrates have the strongest adsorption ability for butyl acetate and methanol. Their adsorption for styrene and xylene is also quite strong. They show weak adsorption performance for benzene molecules and no adsorption effect on n-undecane molecules. Surprisingly, the molecular structure is completely destroyed due to the strong interaction with Ba_2N substrate (Fig. 4r). This significantly demonstrates that Ba_2N is an ideal material for VOCs adsorption. In addition, the equilibrium distance for the adsorption of benzene and n-undecane molecules on the Ba2N substrate is larger than for the other two substrates. However, the adsorption energy for these two molecules on Ba2N is larger than on Ca_2N and Sr_2N. This may result from the higher mass of Ba atoms on the substrate surface. Collectively, these results demonstrate a clear functional-group specificity in adsorption configuration and a strong substrate-dependent variation in adsorption strength.

Mechanism of VOCs adsorption on CaN, SrN, and BaN Surface

Next, we calculate the electronic density of states (DOS) of the Ca_2N substrate when adsorbing VOCs molecules. Figure 5 shows the changes in DOS of VOCs molecules before and after adsorption on a Ca_2N substrate. Briefly, the electronic DOS of Ca_2N has increased in energy compared to the initial energy. However, the DOS of VOCs molecules has decreased in energy compared to the initial state. This indicates that VOCs molecules gain electrons in the reaction, and the Fermi level is relatively higher. Meanwhile, the Ca_2N substrate loses electrons in the reaction, and the Fermi level is relatively lower. Interestingly, the benzene and Ca_2N substrate (Fig. 5a) undergo hybridization in the energy range of -0.5 eV to 2 eV, and the DOS overlaps in this region. Styrene (Fig. 5b), xylene (Fig. 5c), methylbenzene (Fig. 5d), and ethylbenzene (Fig. 5e) exhibit similar orbital hybridization after adsorption on Ca_2N substrates due to their similar structures. The hybridization all occurs in the energy range of -0.5 eV to 2.5 eV and − 4 eV to -3 eV, with some additional hybridization regions compared to benzene. The hybrid orbitals of butyl acetate (Fig. 5f) and methanol (Fig. 5g) adsorbed on a Ca_2N substrate are located in the energy range of -4 eV to -3 eV below the Fermi level. The orbital hybridization of N-undecane (Fig. 5h) after adsorption on the Ca_2N substrate is not significant, indicating that the molecular effect is relatively weak. Besides, the degree of orbital hybridization of VOCs molecules adsorbed on the Ca_2N substrate is consistent with the results of the adsorption energy analysis mentioned earlier. Moreover, the adsorption results of these VOCs molecules on Sr_2N (Fig. 6a-h) and Ba2N (Fig. 7a-h) substrates are similar to those on Ca_2N substrates. They are also consistent with the previous analysis results. Since the molecular structure is completely destroyed, we obtain no DOS for Styrene on Ba_2N (Fig. 7b).

To investigate the charge transfer between VOCs molecules adsorbed on single-layer Ca_2N, Sr_2N, and Ba_2N substrates, we calculate the differential charge density of the adsorbed structure and the amount of charge transferred during the reaction, which is summarized in Table 1. Figure 8 shows the differential charge density of the VOCs molecules adsorbed on a Ca_2N substrate, including top and side views, with

isosurfaces of 0.0015 e/Å for all charge densities. When benzene is adsorbed on a Ca_2N substrate (Fig. 8a), there is a small but significant charge transfer. The substrate part loses electrons on the surface, and the electron loss area is located directly opposite the Ca atom on the other side, slightly higher than the Ca atom at the interface. There is charge accumulation on both sides of the C atom in the benzene molecule, with more charge accumulation on the side closer to the substrate. Charge loss occurs around the H atom, with the lost electrons located on the side farther from the substrate, consistent with the active region in the molecular electrostatic potential. When styrene is adsorbed on Ca_2N substrates (Fig. 8b), there is a significant amount of charge transfer. The region where free electrons accumulate on the substrate surface loses electrons, consistent with the adsorption of benzene molecules. In styrene molecules, there is charge accumulation on both sides of the C atom and charge loss around the H atom. Specifically, the C atom on the C = C bond receives more electrons than the C atom on the benzene ring structure. This indicates that during the adsorption process, both structures interact with electrons on the Ca_2N substrate surface. Among them, the C = C bond undergoes more charge transfer, which is consistent with the results of the geometric structure. Xylene (Fig. 8c), methylbenzene (Fig. 8d), and ethylbenzene (Fig. 8e) all exhibit similar differential charge results when adsorbed on Ca_2N substrates. Overall, they all transfer charges from the Ca_2N substrate to VOCs molecules. Charge loss occurs at the locations where free electrons accumulate on the surface of the Ca_2N substrate, with charge accumulation around Ca atoms at the substrate interface that adsorb xylene and ethylbenzene molecules on the side away from the interface. This arises from charge redistribution caused by charge transfer. The charge gain and loss in molecules mainly occur in the benzene ring structure region. Only a small amount occurs in the alkyl structure region. In addition, when xylene is adsorbed on the Ca_2N substrate, the position of the benzene ring is consistent with that of the benzene molecule. However, for methylbenzene and ethylbenzene, the position of the benzene ring is located directly opposite the Ca atom at the interface. When butyl acetate (Fig. 8f) and methanol (Fig. 8g) are adsorbed on a Ca_2N, there is a significant amount of charge transfer from the substrate to the molecule. The region where free electrons gather in the Ca_2N substrate loses charge. The C and O atoms in the C = O bond of the molecule are charged, and other parts of the molecule also experience charge gain and loss due to charge redistribution. Charge accumulation occurs around Ca atoms on the Ca_2N substrate surface that adsorbs methanal molecules. In the differential charge results of n-undecane adsorption (Fig. 8h), no charge loss occurred at the substrate, indicating that there was no charge transfer between the molecule and the substrate. Collectively, there is no charge transfer between the n-undecane molecule and the Ca_2N substrate. However, other gases have undergone significant charge transfer.

Figure 9 shows the top and side views of the differential charge density after adsorbing VOCs molecules on Sr_2N substrate, with an isosurface of 0.0015 e/Å. Overall, the adsorption results of Sr_2N and Ca_2N substrates are similar, with charges transferred from the substrate to VOCs molecules. The charge transfer amount of benzene (Fig. 9a) and styrene (Fig. 9b) adsorbed on the Sr2N substrate is reduced compared to the Ca2N substrate. In addition, the positions where charges are lost in the substrate are consistent. The charge transfer amount of xylene (Fig. 9c) and methylbenzene (Fig. 9d) molecules

adsorbed on the Sr_2N substrate shows no significant change compared to the Ca_2N substrate. However, the benzene ring structure in the molecules is located directly opposite the Sr atom at the interface. Thus, the position where the charge is lost mainly centered around the Sr atom. The charge transfer amount of ethylbenzene adsorbed on the Sr_2N substrate (Fig. 9e) is significantly reduced compared to the Ca_2N substrate. Besides, the adsorption site also changes. The charge transfer amount of butyl acetate (Fig. 9f) and methanal (Fig. 9g) adsorbed on Sr_2N substrate is similar to that on Ca2N substrate, and the positions of gain and loss electrons are consistent. In Fig. 9h, n-undecane shows no significant charge transfer on the Sr_2N substrate. Concisely, except for changes in the adsorption sites of toluene, xylene, and ethylbenzene, the adsorption characteristics of other molecules on Sr_2N substrates are basically consistent with those on Ca_2N.

Figure 10 shows the top and side views of the differential charge density after adsorbing VOCs molecules on a Ba_2N substrate, with an iso surface of 0.0015 e/Å. Overall, the adsorption results of Ba_2N and Ca_2N substrates are similar, with charges transferred from the substrate to VOCs molecules. The charge transfer amount of benzene (Fig. 10a), xylene (Fig. 10c), methylbenzene (Fig. 10d), and ethylbenzene (Fig. 10e) adsorbed on Ba_2N substrate is reduced compared to the Ca_2N substrate. The adsorption sites of the four molecules are consistent, and the benzene ring structure is located directly above the Ba atoms. Surprisingly, there is a large amount of charge transfer distributed around the scattered atoms after the molecular structure is disrupted (Fig. 10b). The charge transfer amount of butyl acetate (Fig. 10f) and methanal (Fig. 10g) adsorbed on Ba_2N substrate is similar to that on Ca_2N substrate. The n-undecane shows no significant charge transfer on the Ba_2N substrate (Fig. 10h). Collectively, the adsorption of other molecules on the Ba2N substrate is basically the same as that on Ca_2N, except for the structural damage of styrene molecules during adsorption. Based on Table 1 and Figs. 8, 9, and 10, the adsorption of n-undecane molecules on Ca_2N, Sr_2N, and Ba_2N substrates is not significant. Molecules such as xylene, methylbenzene, and ethylbenzene, which are composed of a benzene ring and alkyl structures, have a stronger adsorption capacity. The adsorption of styrene is extremely strong, especially on Ba_2N substrates, which have the ability to damage the molecular structure during the adsorption process.

Electric field improves the adsorption of VOCs to 2D electronic compounds

Given that Ca_2N, Sr_2N, and Ba_2N exhibit weak adsorption toward benzene and n-undecane molecules, they are not readily applicable directly in sensing applications. Therefore, we next introduce regulatory strategies to enhance the adsorption performance of these three substrates. The poor adsorbability of n-undecane molecules arises from the tendency of their surface H atoms to lose electrons, which is incompatible with the abundant free and mobile electrons on the surface of single-layer 2D electronic compounds. For benzene molecules, their weak adsorption performance is attributed to the relatively stable internal structure of the benzene ring. In contrast, its analogous molecules possess additional

functional groups that disrupt the internal stability of the benzene ring. This significantly improves the adsorption efficiency. Among the three substrate materials, Ba_2N demonstrates the weakest overall adsorption performance. Thus, we select benzene as a representative molecule and Ba2N as the substrate to investigate the effect of external regulation on the adsorption capacity.

Common strategies for regulating the adsorption performance of 2D materials include defect engineering, doping modification, electric field regulation, and pressure regulation[50]. Since electric fields can directly modulate the free electrons on the substrate surface, we employ an electric field applied along the z-axis for regulation. We simulate an external electric field and calculate the adsorption behavior of benzene molecules on the substrate under electric fields ranging from − 0.8 eV/Å to 0.8 eV/Å along the z-axis, with an interval of 0.2 eV/Å. Figure 11a&b show the differential charge density maps of benzene adsorbed on the substrate under electric fields of varying intensities. Figure 11c depicts the variation curves of charge transfer and equilibrium distance for benzene adsorption on the substrate under different electric field conditions. As shown in Fig. 11b, when an electric field of − 0.2 to − 0.8 eV/Å is applied, the electrons in the system experience a downward electric field force, which hinders the transfer of free electrons from the substrate surface to the molecule and also impedes the redistribution of charge within the molecule, resulting in a reduction in charge transfer. When an electric field of 0.2 to 1.0 eV/Å is applied, the electrons in the system are subjected to an upward electric field force, which facilitates the transfer of free electrons from the substrate surface to the molecule. Meanwhile, the direction of charge redistribution within the molecule aligns with the direction of the electric field force, promoting the formation of a new equilibrium and thus increasing charge transfer. Figure 11c visualizes the variation patterns of charge transfer and equilibrium distance. Within the range of 0.8 eV/Å, as the intensity of the electric field applied downward along the z-axis increases, the charge transfer increases while the equilibrium distance decreases. This indicates a linear relationship between the electric field and the sensing performance of the substrate. However, beyond 0.8 eV/Å, increasing the electric field intensity leads to a decrease in charge transfer and an increase in equilibrium distance. These results collectively indicate that the electric field modulates the adsorption interaction between VOCs molecules and the substrate material by altering the distribution and movement tendency of electrons.

Conclusion

We show that Ca_2N, Sr_2N, and Ba_2N provide effective adsorption for VOCs. Ca_2N, Sr_2N, and Ba_2N have adsorption effects on benzene, styrene, xylene, methylbenzene, ethylbenzene, butyl acetate, and methanal. All adsorption processes do not damage the structure of the substrate materials. Thus, the substrate can be reused. Surprisingly, the molecular structure of styrene adsorbs on Ba_2N is destroyed due to strong interactions. Benzene and n-undecane adsorb mainly through van der Waals forces due to their low charge transfer. The adsorption energy and charge transfer amount of styrene containing a C = C bond and a benzene ring structure are the highest. Xylene, methylbenzene, and ethylbenzene, which contain benzene ring structures or C = O bonds, follow closely behind. The adsorption effect of benzene still exhibits significant adsorption energy and charge transfer. The adsorption effect of N-undecane is

the worst. Especially, the application of an electric field in the z-direction significantly improves the ability of Ba_2N to adsorb benzene. Our research can be used to effectively adsorb VOCs and control air pollution. In addition, the alkali metal nitrides used in the experiment and the method of applying an electric field provide new ideas for exploring other adsorption materials. Subsequent research can use doping, defects, and other methods to compare their adsorption effects, and it is worthwhile to make VOCs sensors based on Ca_2N, Sr_2N, and Ba_2N.

Methods

DFT-based first-principles calculations were performed with a plane-wave basis set as implemented in the Vienna ab initio simulation package (VASP)[51]. The projector augmented wave method was employed to describe the ion–electron interaction[52]. The exchange correlation functional used in the calculation is PBE functional in GGA[53], and the pseudopotential is PAW. The truncation energy based on plane waves is set to 400 eV. During the modeling process, a 25 Å vacuum layer is added to eliminate the mutual influence between periodic unit cells in the z-direction, in order to simulate the structure of a single layer. The initial structure is a 1 × 1 single-layer structure on the xy plane. In order to prevent mutual influence between adjacent unit cells in the plane and maintain sufficient distance between each molecule, the substrate structure was expanded to 3 × 3 × 1 when constructing the adsorption model. In the structural optimization, the total energy was set to converge to 10 − 5 eV, and the force on each atom converged to 0.01 eV/Å before stopping relaxation. The K-point sampling grid was set to 7 × 7 × 1. In electronic structure calculation, the accuracy of K-point sampling grid is improved to 9 × 9 × 1. In addition, in order to eliminate the influence of van der Waals forces in the calculation, the DFT-D3 method was used for van der Waals force correction in each step of the calculation.

The adsorption energy (Ea) of different molecules on Ca2N, Sr2N, and Ba2N surfaces was computed, in which Ea can be expressed by,

$Ea = Etotal - (Em + Esur)$

where Etotal is the total energy of the adsorbed system. Em and Esur are the

energies of relaxed molecules in the gas phase and on the Ca2N, Sr2N, and Ba2N surfaces, respectively. By this definition, larger negative values of Ea denote stronger interaction between the molecule and the surface.

Declarations

Competing interests

All authors declare no financial or non-financial competing interests.

Author Contribution

JW performed the DFT study. XZ analyzed the data. QC & SL are contributors in writing the manuscript. MZ & QC design and supervise this study. All authors read and approved the final manuscript.

Acknowledgements

This work was supported by grants from the Natural Science Foundation of Chongqing (CSTB2023NSCQ-MSX0620) .

Data Availability

All data generated or analysed during this study are included in this published article.

References

1 Feng, Y. L., Yang, C. & Cao, X. L. Intermediate volatile organic compounds in Canadian residential air in winter: Implication to indoor air quality. *Chemosphere* **328** (2023). https://doi.org/ARTN 138567

10.1016/j.chemosphere.2023.138567

2 Corbasson, I., Hankinson, S. E., Stanek, E. J. & Reeves, K. W. Urinary bisphenol-A, phthalate metabolites and body composition in US adults, NHANES 1999-2006. *Int J Environ Heal R* **26**, 606-617 (2016). https://doi.org/10.1080/09603123.2016.1233524

3 Zhou, X., Zhou, X., Wang, C. & Zhou, H. Environmental and human health impacts of volatile organic compounds: A perspective review. *Chemosphere* **313**, 137489 (2023). https://doi.org/10.1016/j.chemosphere.2022.137489

4 Alwis, K. U., Blount, B. C., Britt, A. S., Patel, D. & Ashley, D. L. Simultaneous analysis of 28 urinary VOC metabolites using ultra high performance liquid chromatography coupled with electrospray ionization tandem mass spectrometry (UPLC-ESI/MSMS). *Anal Chim Acta* **750**, 152-160 (2012). https://doi.org/10.1016/j.aca.2012.04.009

5 Manisalidis, I., Stavropoulou, E., Stavropoulos, A. & Bezirtzoglou, E. Environmental and Health Impacts of Air Pollution: A Review. *Front Public Health* **8**, 14 (2020). https://doi.org/10.3389/fpubh.2020.00014

6 Arias-Perez, R. D. *et al.* Inflammatory effects of particulate matter air pollution. *Environ Sci Pollut Res Int* **27**, 42390-42404 (2020). https://doi.org/10.1007/s11356-020-10574-w

7 Wang, J. *et al.* Long-Term Exposure to Low Concentrations of Ambient Benzene and Mortality in a National English Cohort. *Am J Respir Crit Care Med* **209**, 987-994 (2024).

https://doi.org/10.1164/rccm.202308-1440OC

8 Liu, X. L. *et al.* Association of volatile organic compound levels with chronic obstructive pulmonary diseases in NHANES 2013-2016. *Sci Rep-Uk* **14** (2024). https://doi.org/ARTN 16085

10.1038/s41598-024-67210-7

9 Shala, N. K. *et al.* Exposure to benzene and other hydrocarbons and risk of bladder cancer among male offshore petroleum workers. *Br J Cancer* **129**, 838-851 (2023). https://doi.org/10.1038/s41416-023-02357-0

10 Guo, J. H. *et al.* Environmental Toxicant Exposure and Depressive Symptoms. *Jama Netw Open* **7** (2024). https://doi.org/ARTN e2420259

10.1001/jamanetworkopen.2024.20259

11 Tang, L., Liu, M. & Tian, J. Volatile organic compounds exposure associated with depression among U.S. adults: Results from NHANES 2011-2020. *Chemosphere* **349**, 140690 (2024). https://doi.org/10.1016/j.chemosphere.2023.140690

12 Ren, J. *et al.* Exposure to volatile organic compounds and growth indicators in adolescents: Unveiling the association and potential intervention strategies. *J Hazard Mater* **477**, 135422 (2024). https://doi.org/10.1016/j.jhazmat.2024.135422

13 Meng, L., Wang, Y., Wang, X., Mu, M. & Zheng, H. Association between exposure to volatile organic compounds and atherogenic index of plasma in NHANES 2011-2018. *Sci Rep* **15**, 9024 (2025). https://doi.org/10.1038/s41598-025-93833-5

14 Feng, X. *et al.* Exposure to volatile organic compounds and mortality in US adults: A population-based prospective cohort study. *Sci Total Environ* **928**, 172512 (2024). https://doi.org/10.1016/j.scitotenv.2024.172512

15 Moura, P. C., Raposo, M. & Vassilenko, V. Breath volatile organic compounds (VOCs) as biomarkers for the diagnosis of pathological conditions: A review. *Biomed J* **46**, 100623 (2023). https://doi.org/10.1016/j.bj.2023.100623

16 Xu, W. *et al.* Rapid screen for ventilator associated pneumonia using exhaled volatile organic compounds. *Talanta* **253** (2023). https://doi.org/10.1016/j.talanta.2022.124069

17 Ge, D. *et al.* Analysis of volatile organic compounds in exhaled breath after radiotherapy. *J Zhejiang Univ Sci B* **23**, 153-157 (2022). https://doi.org/10.1631/jzus.B2100447

18 Zhu, L., Shen, D. & Luo, K. H. A critical review on VOCs adsorption by different porous materials: Species, mechanisms and modification methods. *J Hazard Mater* **389**, 122102 (2020).

https://doi.org/10.1016/j.jhazmat.2020.122102

19 Zhang, X. Y., Gao, B., Creamer, A. E., Cao, C. C. & Li, Y. C. Adsorption of VOCs onto engineered carbon materials: A review. *Journal of Hazardous Materials* **338**, 102-123 (2017). https://doi.org/10.1016/j.jhazmat.2017.05.013

20 Ye, Q. *et al.* Management of typical VOCs in air with adsorbents: status and challenges. *Dalton Trans* **52**, 12169-12184 (2023). https://doi.org/10.1039/d3dt01930f

21 Wang, S., Zhang, L., Long, C. & Li, A. Enhanced adsorption and desorption of VOCs vapor on novel micro-mesoporous polymeric adsorbents. *J Colloid Interface Sci* **428**, 185-190 (2014). https://doi.org/10.1016/j.jcis.2014.04.055

22 Serna-Guerrero, R. & Sayari, A. Applications of pore-expanded mesoporous silica. 7. Adsorption of volatile organic compounds. *Environ Sci Technol* **41**, 4761-4766 (2007). https://doi.org/10.1021/es0627996

23 Mcdonald, S. R. & Tao, S. Q. An optical fiber chlorogenic acid sensor using a Chitosan membrane coated bent optical fiber probe. *Analytica Chimica Acta* **1288** (2024). https://doi.org/ARTN 342142

10.1016/j.aca.2023.342142

24 Grate, J. W. & Zellers, E. T. The fractional free volume of the sorbed vapor in modeling the viscoelastic contribution to polymer-coated surface acoustic wave vapor sensor responses. *Anal Chem* **72**, 2861-2868 (2000). https://doi.org/10.1021/ac991192n

25 Jahandar Lashaki, M. *et al.* The role of beaded activated carbon's pore size distribution on heel formation during cyclic adsorption/desorption of organic vapors. *J Hazard Mater* **315**, 42-51 (2016). https://doi.org/10.1016/j.jhazmat.2016.04.071

26 Wang, H. *et al.* Functionalized hollow siliceous spheres for VOCs removal with high efficiency and stability. *J Hazard Mater* **268**, 115-123 (2014). https://doi.org/10.1016/j.jhazmat.2013.12.070

27 Zhu, L. L., Shen, D. K. & Luo, K. H. A critical review on VOCs adsorption by different porous materials: Species, mechanisms and modification methods. *Journal of Hazardous Materials* **389** (2020). https://doi.org/ARTN 122102

10.1016/j.jhazmat.2020.122102

28 Deng, L. L. *et al.* Effects of microstructure of clay minerals, montmorillonite, kaolinite and halloysite, on their benzene adsorption behaviors. *Appl Clay Sci* **143**, 184-191 (2017). https://doi.org/10.1016/j.clay.2017.03.035

29 Muir, B., Sobczyk, M. & Bajda, T. Fundamental features of mesoporous functional materials influencing the efficiency of removal of VOCs from aqueous systems: A review. *Science of the Total Environment* **784** (2021). https://doi.org/ARTN 147121

10.1016/j.scitotenv.2021.147121

30 Gan, G., Fan, S., Li, X., Zhang, Z. & Hao, Z. Adsorption and membrane separation for removal and recovery of volatile organic compounds. *J Environ Sci (China)* **123**, 96-115 (2023). https://doi.org/10.1016/j.jes.2022.02.006

31 Li, X. Q. *et al.* Adsorption materials for volatile organic compounds (VOCs) and the key factors for VOCs adsorption process: A review. *Sep Purif Technol* **235** (2020). https://doi.org/ARTN 116213

10.1016/j.seppur.2019.116213

32 Xie, Y., Lyu, S., Zhang, Y. & Cai, C. Adsorption and Degradation of Volatile Organic Compounds by Metal-Organic Frameworks (MOFs): A Review. *Materials (Basel)* **15** (2022). https://doi.org/10.3390/ma15217727

33 Ye, Q. Q. *et al.* Management of typical VOCs in air with adsorbents: status and challenges. *Dalton T* **52**, 12169-12184 (2023). https://doi.org/10.1039/d3dt01930f

34 Muir, B., Sobczyk, M. & Bajda, T. Fundamental features of mesoporous functional materials influencing the efficiency of removal of VOCs from aqueous systems: A review. *Sci Total Environ* **784**, 147121 (2021). https://doi.org/10.1016/j.scitotenv.2021.147121

35 Cheng, M. Q. *et al.* Penta-Graphene as a Potential Gas Sensor for NO

Detection. *Nanoscale Res Lett* **14** (2019). https://doi.org/ARTN 306

10.1186/s11671-019-3142-4

36 Wang, H. N. *et al.* Functionalized hollow siliceous spheres for VOCs removal with high efficiency and stability. *Journal of Hazardous Materials* **268**, 115-123 (2014). https://doi.org/10.1016/j.jhazmat.2013.12.070

37 Kumari, S., Dalal, J., Kumar, V., Kumar, A. & Ohlan, A. Emerging Two-Dimensional Materials for Electromagnetic Interference Shielding Application. *Int J Mol Sci* **24** (2023). https://doi.org/ARTN 12267

10.3390/ijms241512267

38 Siao, M. D. *et al.* Two-dimensional electronic transport and surface electron accumulation in MoS. *Nat Commun* **9** (2018). https://doi.org/ARTN 1442

10.1038/s41467-018-03824-6

39 Mounet, N. *et al.* Two-dimensional materials from high-throughput computational exfoliation of experimentally known compounds. *Nat Nanotechnol* **13**, 246-+ (2018). https://doi.org/10.1038/s41565-017-0035-5

40 Zavabeti, A. *et al.* Two-Dimensional Materials in Large-Areas: Synthesis, Properties and Applications. *Nano-Micro Lett* **12** (2020). https://doi.org/ARTN 66

10.1007/s40820-020-0402-x

41 Chen, J. H., Xiong, Y. F., Xu, F. & Lu, Y. Q. Silica optical fiber integrated with two-dimensional materials: towards opto-electro-mechanical technology. *Light-Sci Appl* **10** (2021). https://doi.org/ARTN 78

10.1038/s41377-021-00520-x

42 Lee, K., Kim, S. W., Toda, Y., Matsuishi, S. & Hosono, H. Dicalcium nitride as a two-dimensional electride with an anionic electron layer. *Nature* **494**, 336-340 (2013). https://doi.org/10.1038/nature11812

43 Oh, J. S. *et al.* Evidence for Anionic Excess Electrons in a Quasi-Two-Dimensional Ca2N Electride by Angle-Resolved Photoemission Spectroscopy. *J Am Chem Soc* **138**, 2496-2499 (2016). https://doi.org/10.1021/jacs.5b12668

44 Oh, J. S. *et al.* Evidence for Anionic Excess Electrons in a Quasi-Two-Dimensional Ca

N Electride by Angle-Resolved Photoemission Spectroscopy. *Journal of the American Chemical Society* **138**, 2496-2499 (2016). https://doi.org/10.1021/jacs.5b12668

45 Guan, S., Yang, S. Y. A., Zhu, L. Y., Hu, J. P. & Yao, Y. G. Electronic, Dielectric, and Plasmonic Properties of Two-Dimensional Electride Materials X

N (X=Ca, Sr): A First-Principles Study. *Sci Rep-Uk* **5** (2015). https://doi.org/ARTN 12285

10.1038/srep12285

46 Gonzalez, M. I. *et al.* Separation of Xylene Isomers through Multiple Metal Site Interactions in Metal-Organic Frameworks. *J Am Chem Soc* **140**, 3412-3422 (2018). https://doi.org/10.1021/jacs.7b13825

47 Daza, E. E., Maza, J. & Torres, R. Molecular Electrostatic Potential as a Graph. *Curr Comput-Aid Drug* **9**, 272-280 (2013). https://doi.org/Doi 10.2174/1573409911309020011

48 Shin, D. & Jung, Y. Molecular electrostatic potential as a general and versatile indicator for electronic substituent effects: statistical analysis and applications. *Phys Chem Chem Phys* **24**, 25740-25752 (2022). https://doi.org/10.1039/d2cp03244a

49 Galabov, B., Nikolova, V. & Ilieva, S. Does the Molecular Electrostatic Potential Reflect the Effects of Substituents in Aromatic Systems? *Chem-Eur J* **19**, 5149-5155 (2013). https://doi.org/10.1002/chem.201204092

50 Yang, S. L. *et al.* A DFT study of CO adsorption on the pristine, defective, In-doped and Sb-doped graphene and the effect of applied electric field. *Appl Surf Sci* **480**, 205-211 (2019). https://doi.org/10.1016/j.apsusc.2019.02.244

51 Kresse, G. & Furthmuller, J. Efficient iterative schemes for ab initio total-energy calculations using a plane-wave basis set. *Phys Rev B Condens Matter* **54**, 11169-11186 (1996). https://doi.org/10.1103/physrevb.54.11169

52 Blochl, P. E. Projector augmented-wave method. *Phys Rev B Condens Matter* **50**, 17953-17979 (1994). https://doi.org/10.1103/physrevb.50.17953

53 Perdew, J. P., Burke, K. & Ernzerhof, M. Generalized Gradient Approximation Made Simple. *Phys Rev Lett* **77**, 3865-3868 (1996). https://doi.org/10.1103/PhysRevLett.77.3865

Tables

Table.1 Adsorption energy, charge transfer amount and equilibrium distance of benzene, styrene, xylene, methylbenzene, ethylbenzene, butyl acetate, methanal, and n-undecane adsorbed by Ca2N, Sr2N, and Ba2N.

	Ca_2N			Sr_2N			Ba_2N		
	d/Å	△*E*/eV	△*q*/*e*	*d*/Å	△*E*/eV	△*q*/*e*	*d*/Å	△*E*/eV	△*q*/*e*
Benzene	2.66	-0.83	0.95	2.70	-0.71	0.77	2.93	-0.79	0.79
Styrene	1.78	-2.75	2.11	1.86	-2.53	1.80	0.87	2.17	5.11
Xylene	2.00	-1.54	1.81	1.85	-1.41	1.72	2.54	-0.89	0.91
Methylbenzene	1.89	-1.67	1.74	1.88	-1.36	1.70	2.89	-0.87	0.87
Ethylbenzene	1.90	-1.59	1.84	2.25	-0.83	1.00	2.51	-0.95	0.96
Butyl acetate	1.14	-2.07	1.73	1.25	-1.66	1.63	1.47	-1.25	1.38
Methanal	1.07	-3.21	1.60	1.14	-2.89	1.61	1.32	-2.52	1.48
N-undecane	2.97	-0.60	0.64	2.96	-0.62	0.67	2.96	-0.75	0.61

Figures

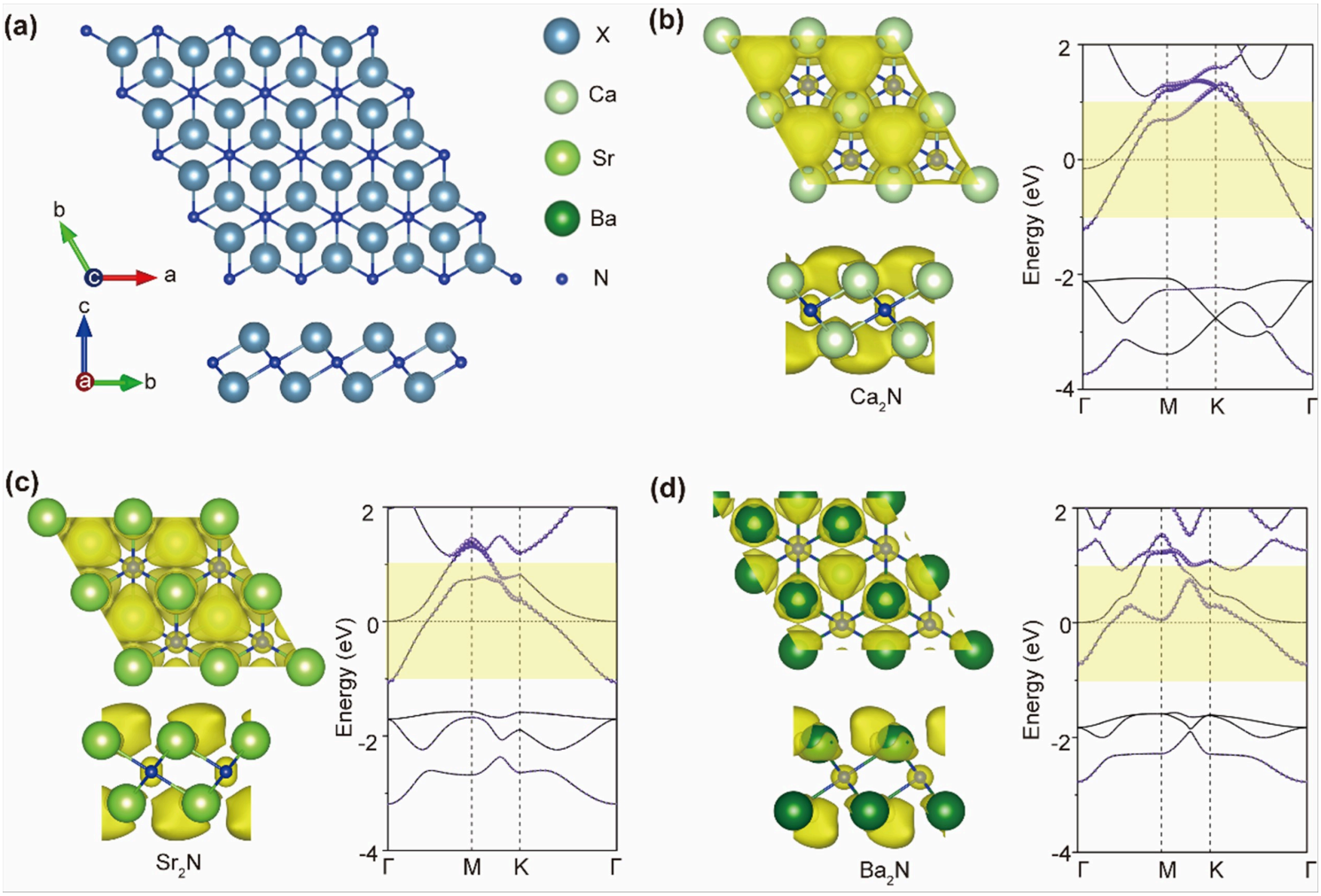


Figure 1

(a) Geometric structures of 2D electronic compounds Ca2N, Sr2N, and Ba2N.X represents Ca, Sr, and Ba. Each X atom is bonded to three adjacent N atoms, and each N atom is bonded to six adjacent X atoms. (b) Ca2N local charge density map and projected energy band. (c) Sr2N local charge density map and projected energy band. (d) Ba2N local charge density map and projected energy band. The purple circle in the band diagram represents the projected band of free electrons, and the yellow area represents the range corresponding to the local charge density map. The Fermi level is set to 0. The isosurface is set to 0.01e/A.

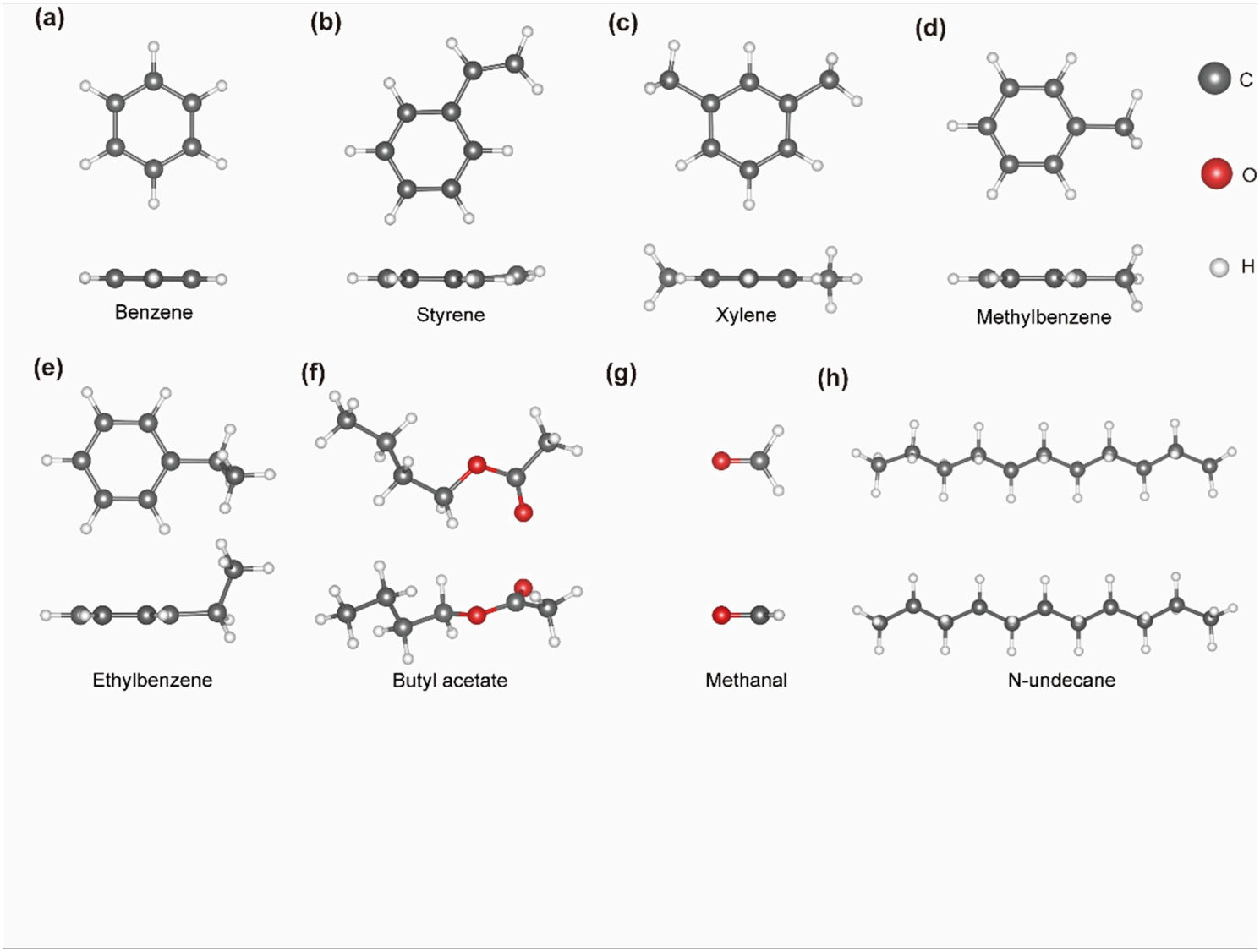


Figure 2

(a)~(h) Top view and side view of benzene, styrene, xylene, methylbenzene, ethylbenzene, butyl acetate, methanal, and n-undecane. The gray ball represents C, the red ball represents O, and the white ball represents H.

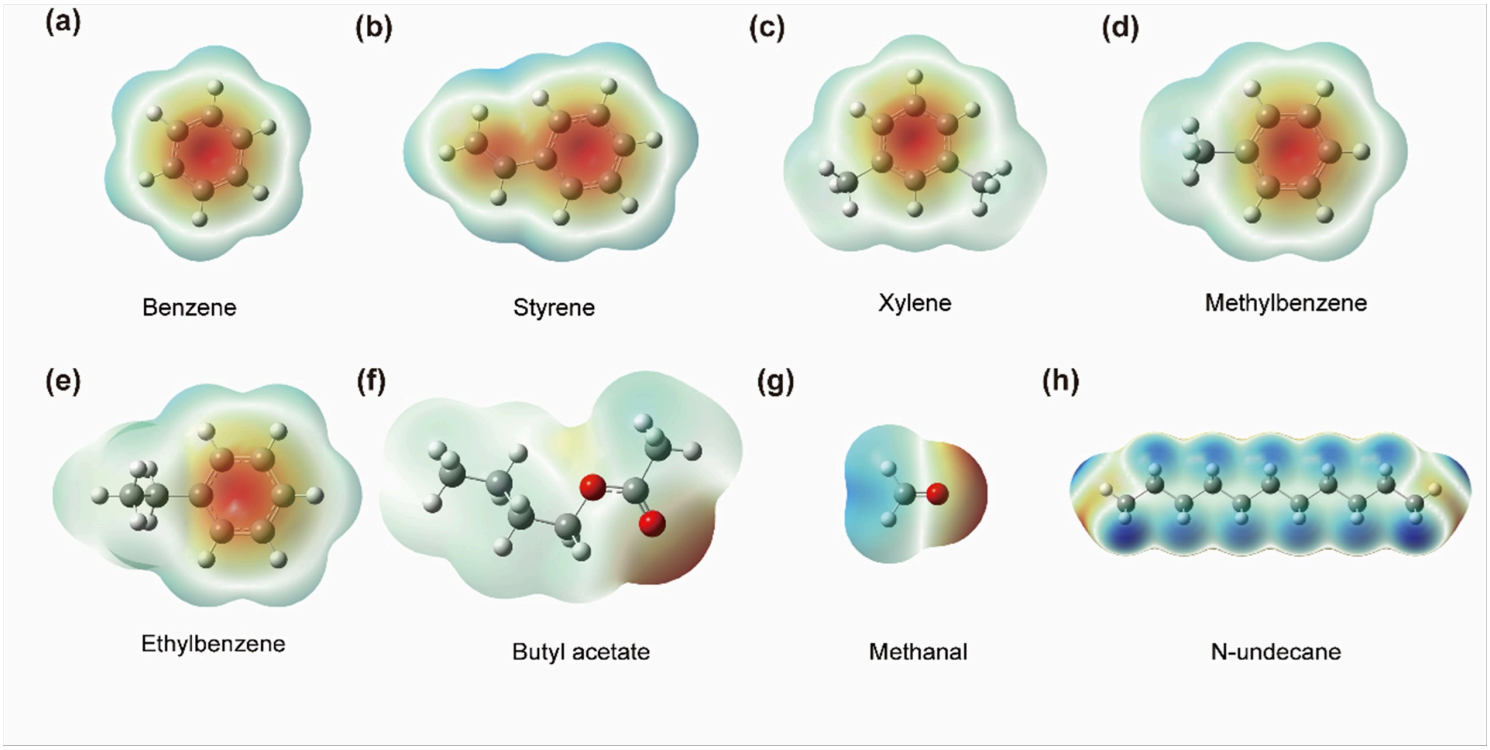


Figure 3

Molecular electrostatic potential of benzene (a), styrene (b), xylene (c), methylbenzene (d), ethylbenzene (e), butyl acetate (f), methanal (g), and n-undecane (h). The red area indicates low energy and easy access to electrons, while both the red and blue areas represent more active areas on the surface of the molecule.

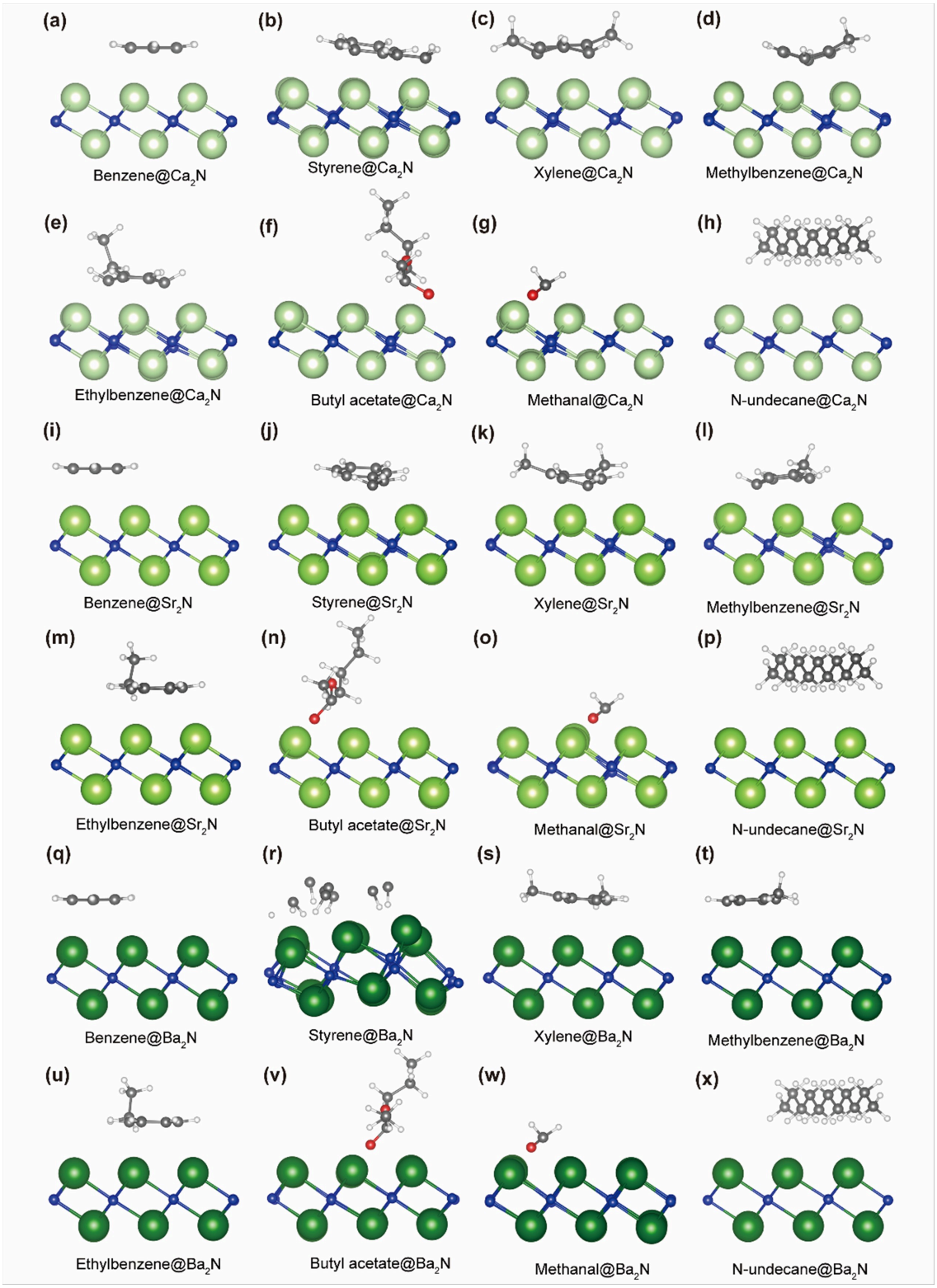


Figure 4

Side view of the combined structure of benzene, styrene, xylene, methylbenzene, ethylbenzene, butyl acetate, methanal, n-undecane with three electrides (Ca2N, Sr2N, Ba2N) substrates after structural relaxation. The gray ball represents C, the red ball represents O, and the white ball represents H. The light green, green and dark green balls represent Ca, Sr, and Ba, respectively. The blue ball represents N.

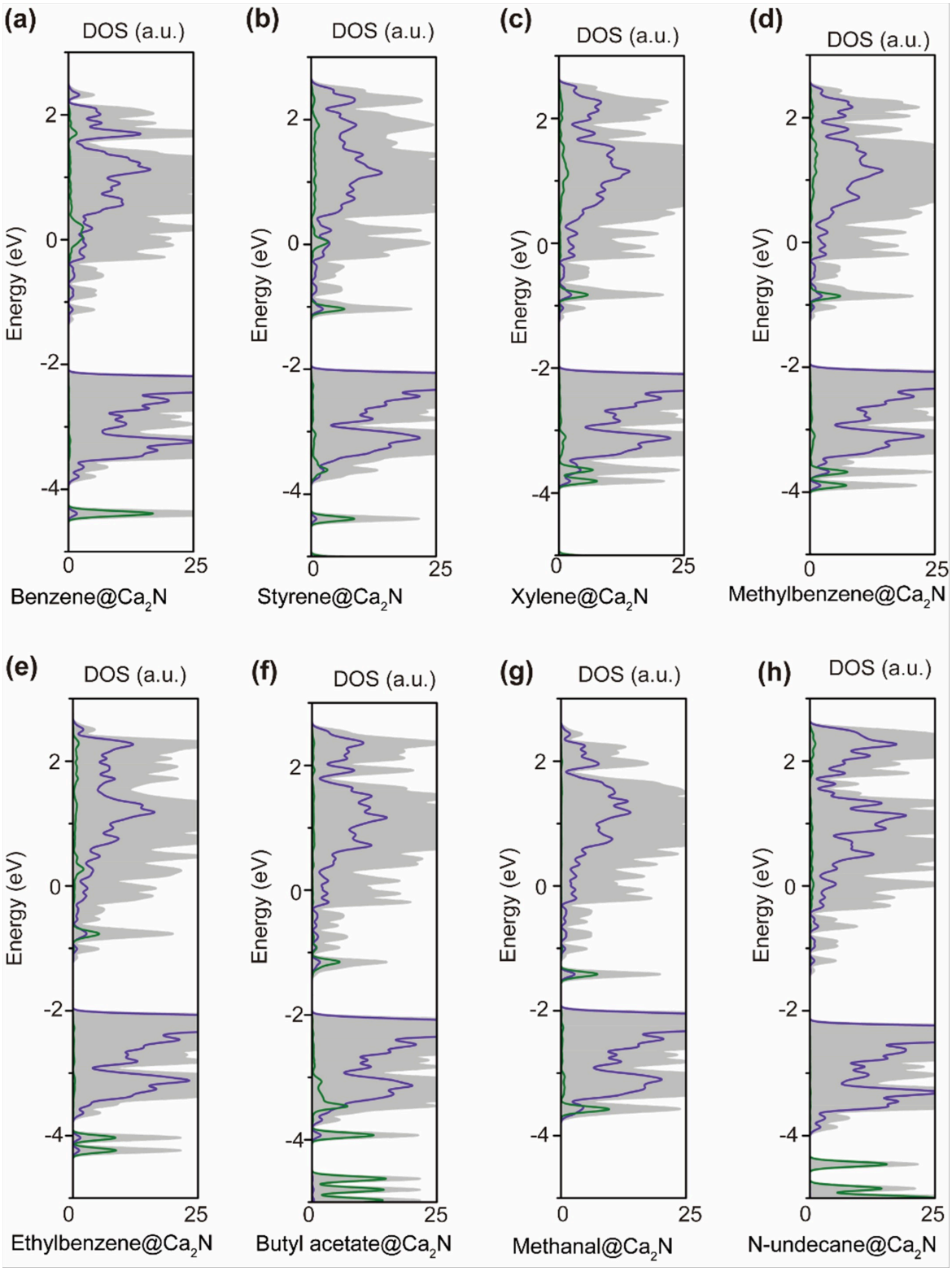


Figure 5

The partial wave electron state density of the combination of benzene (a), styrene (b), xylene (c), methylbenzene (d), ethylbenzene (e), butyl acetate (f), methanal (g), and n-undecane (h) on the Ca_2N substrate after structural relaxation. The gray shadow represents the state density of the Ca_2N substrate after adsorption. The green line represents the state density of VOCs molecules after adsorption, and the purple line represents the state density of VOCs molecules before adsorption.

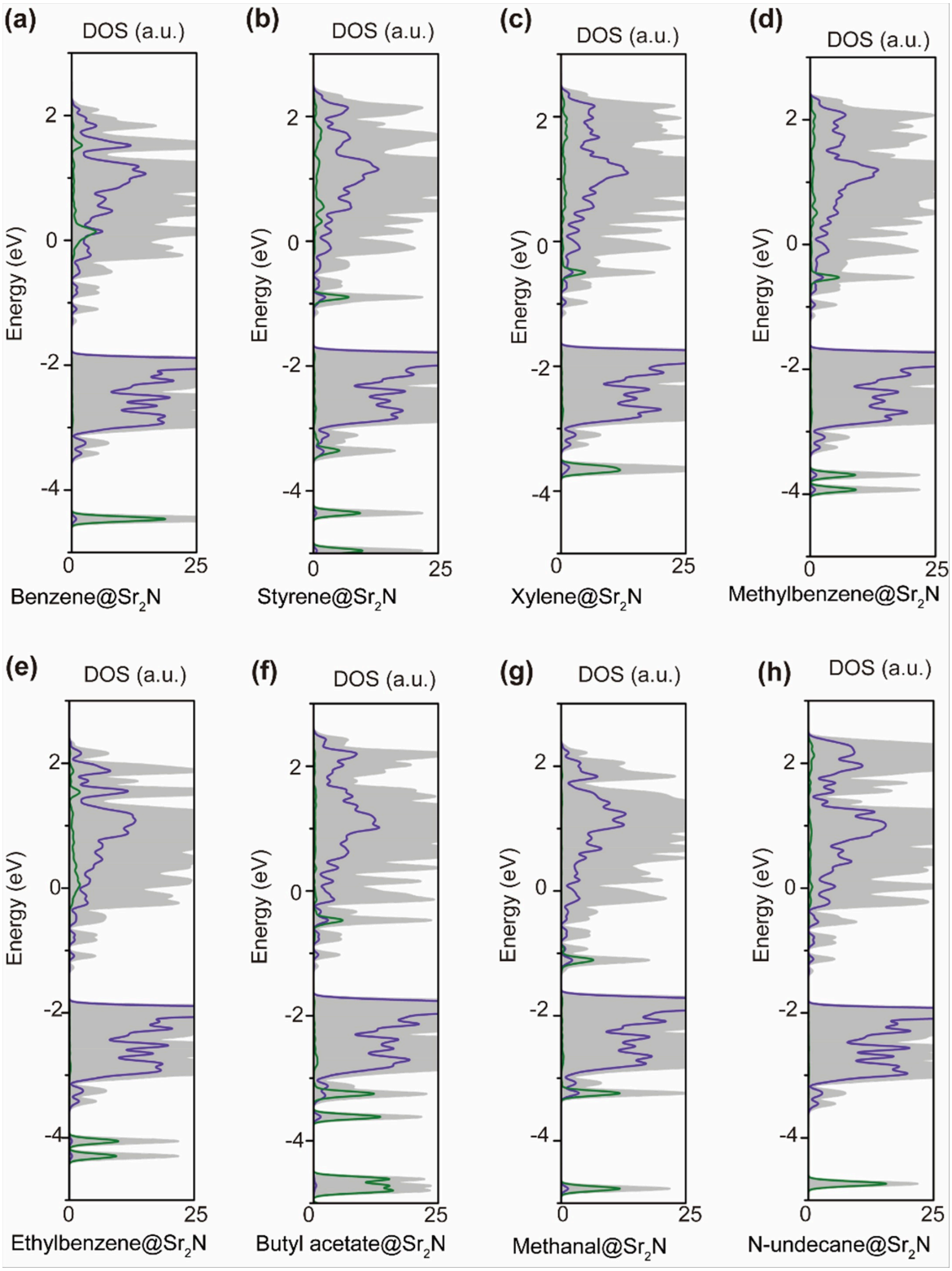


Figure 6

The partial wave electron state density of the combination of benzene (a), styrene (b), xylene (c), methylbenzene (d), ethylbenzene (e), butyl acetate (f), methanal (g), and n-undecane (h) on Sr_2N substrate after structural relaxation. The gray shadow represents the state density of the Sr_2N substrate

after adsorption. The green line represents the state density of VOCs molecules after adsorption, and the purple line represents the state density of VOCs molecules before adsorption.

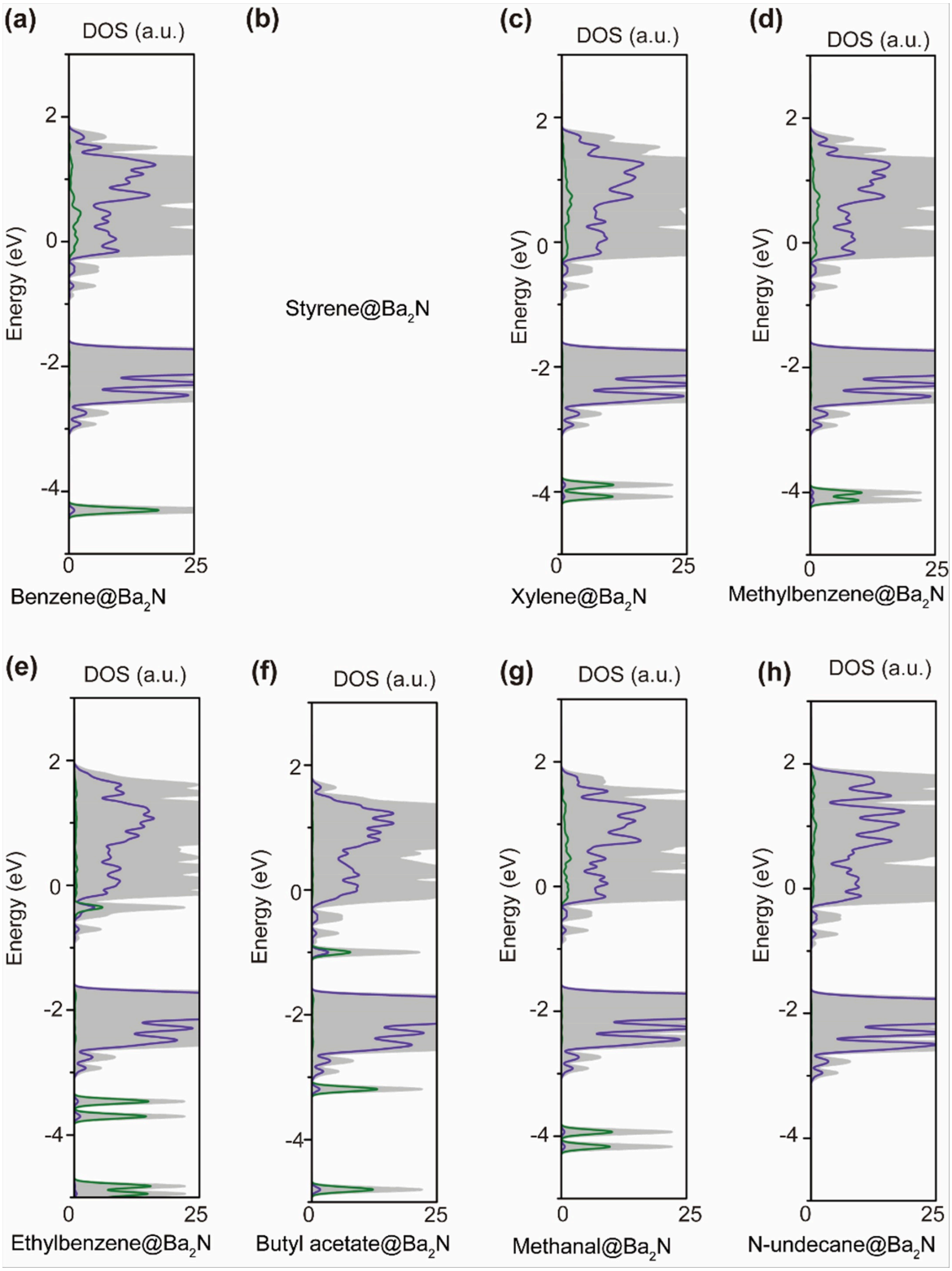


Figure 7

The partial wave electron state density of the combination of benzene (a), styrene (b), xylene (c), methylbenzene (d), ethylbenzene (e), butyl acetate (f), methanal (g), and n-undecane (h) on Ba_2N substrate after structural relaxation. The gray shadow represents the state density of the Ba_2N substrate after adsorption. The green line represents the state density of VOCs molecules after adsorption, and the purple line represents the state density of VOCs molecules before adsorption.

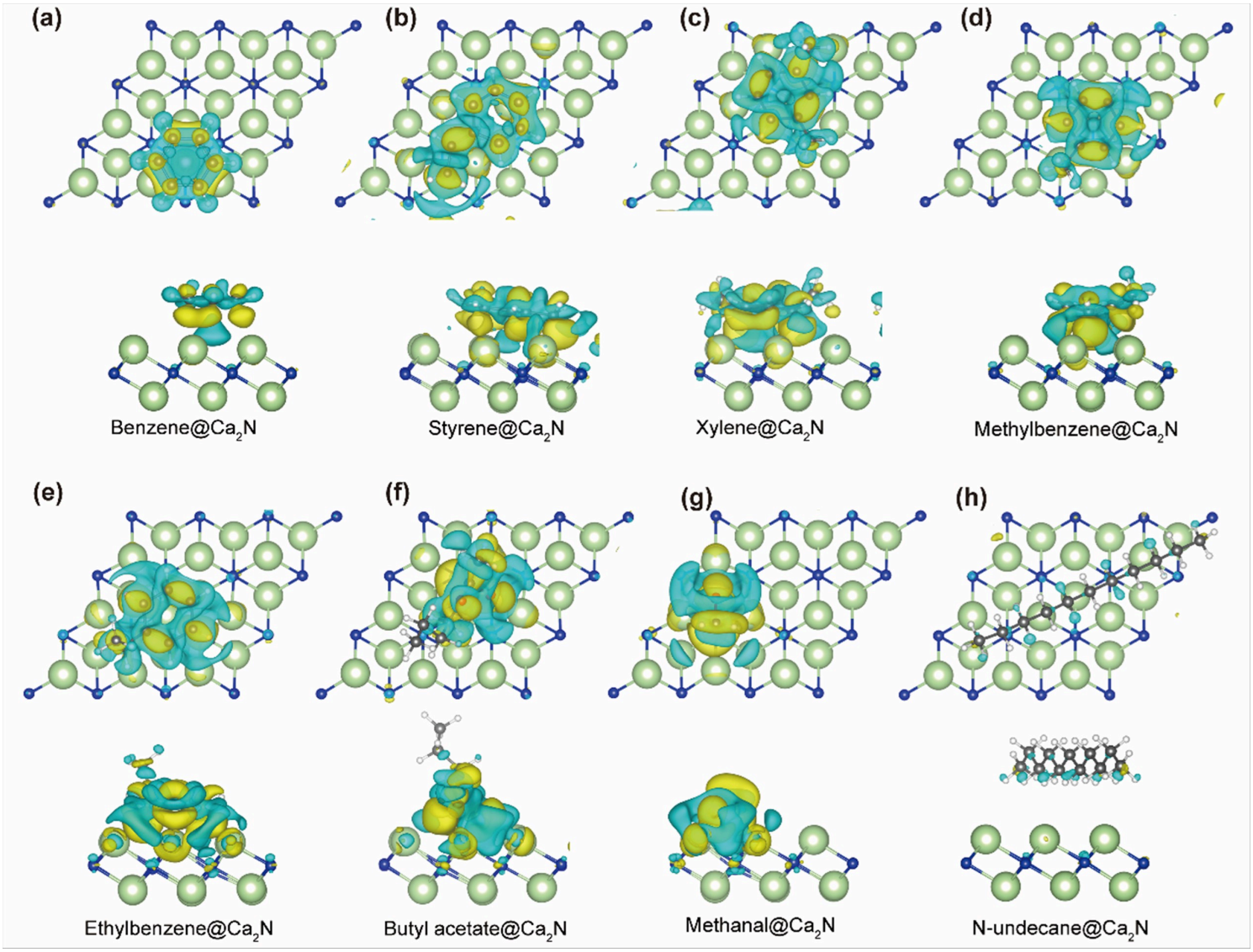


Figure 8

Top view and side view of differential charge density diagram of benzene (a), styrene (b), xylene (c), methylbenzene (d), ethylbenzene (e), butyl acetate (f), methanal (g), and n-undecane (h) combined with Ca_2N substrate. The isosurface is set to 0.0015e/A. The yellow area represents charge accumulation and the blue area represents charge depletion.

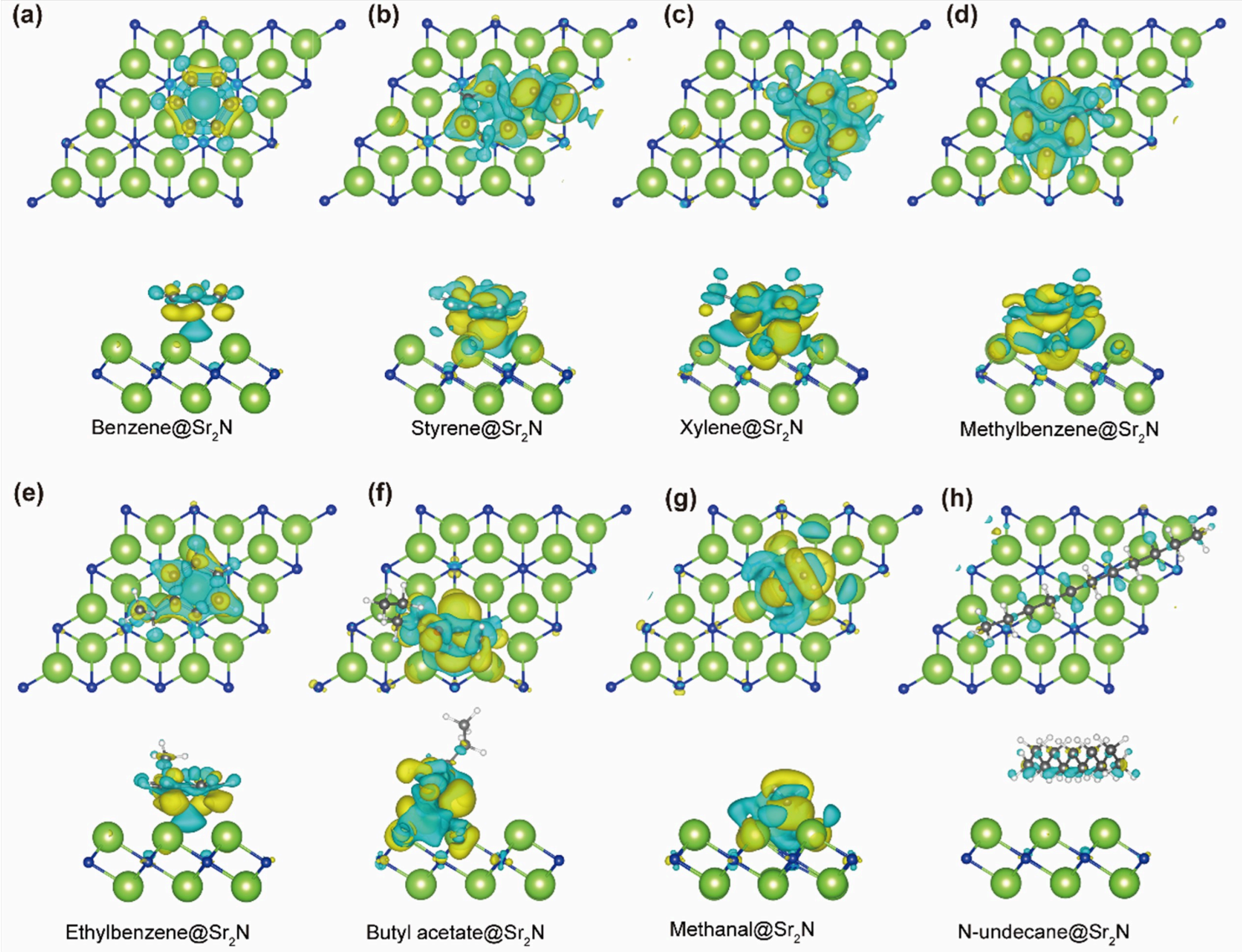


Figure 9

Top view and side view of differential charge density diagram of benzene (a), styrene (b), xylene (c), methylbenzene (d), ethylbenzene (e), butyl acetate (f), methanal (g), and n-undecane (h) combined with Sr_2N substrate. The isosurface is set to 0.0015e/A. The yellow area represents charge accumulation and the blue area represents charge depletion.

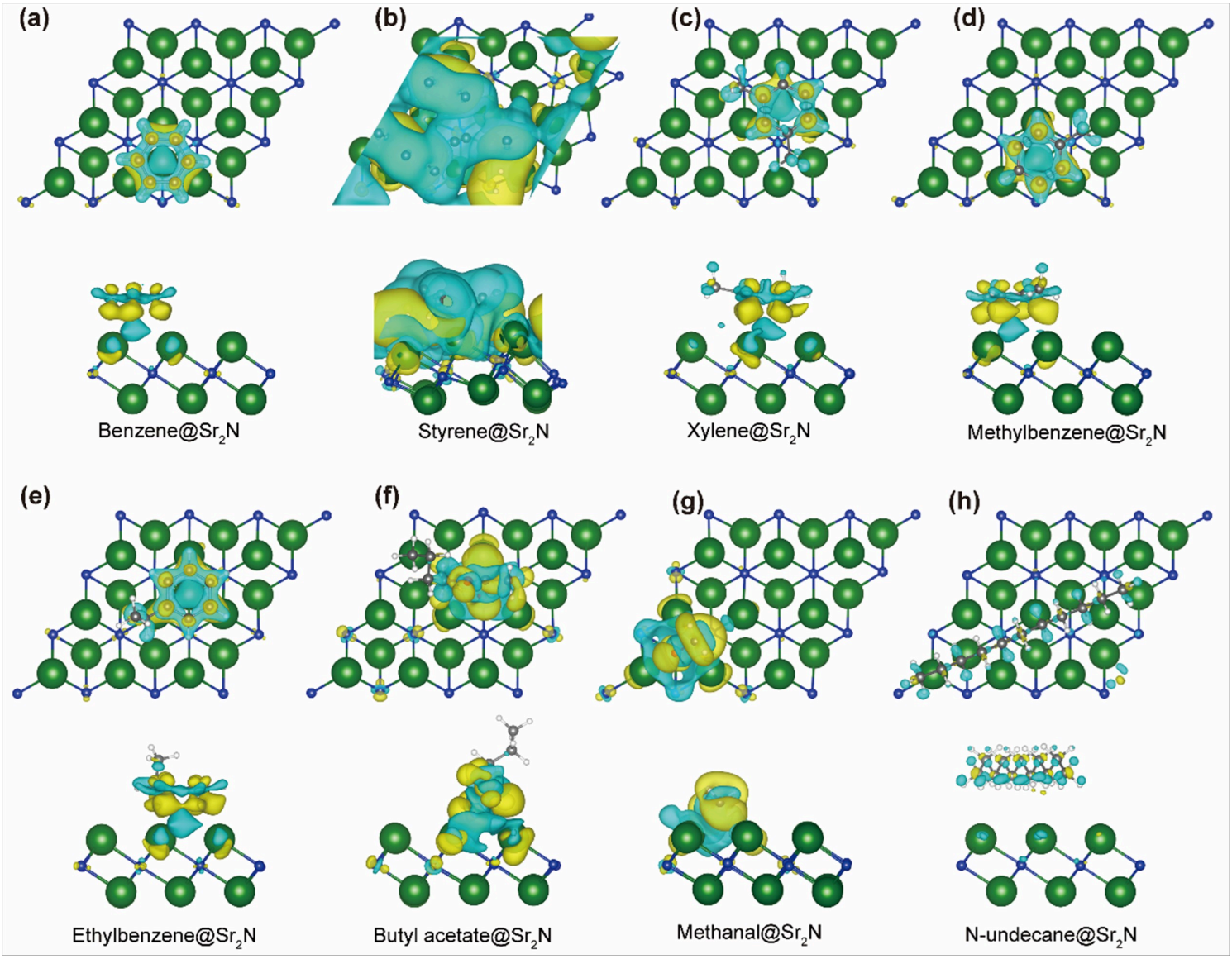


Figure 10

Top view and side view of differential charge density diagram of benzene (a), styrene (b), xylene (c), methylbenzene (d), ethylbenzene (e), butyl acetate (f), methanal (g), and n-undecane (h) combined with Ba_2N substrate. The isosurface is set to 0.0015e/A. The yellow area represents charge accumulation and the blue area represents charge depletion.

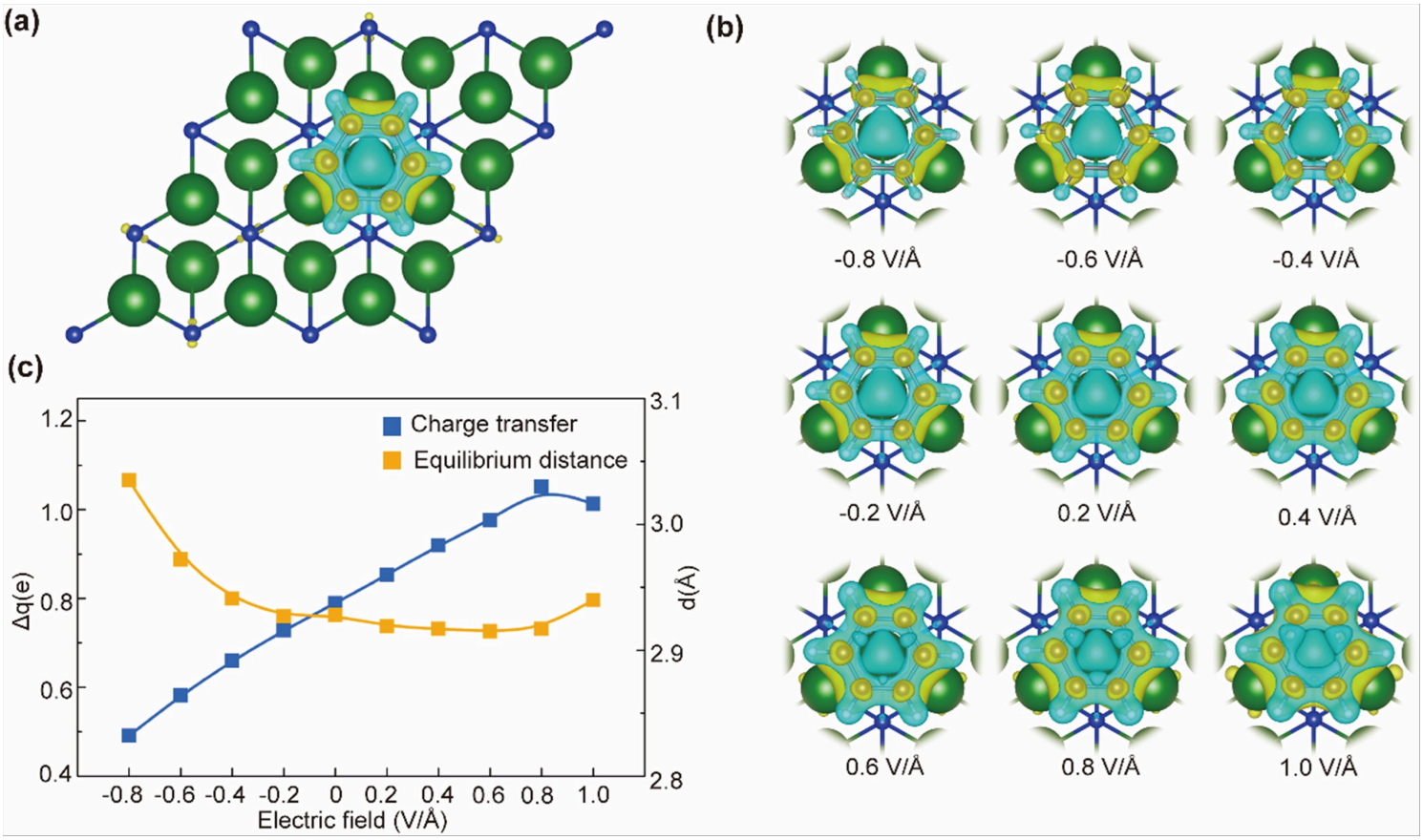


Figure 11

(a) The differential charge density maps of benzene molecules adsorbed on the Ba_2N substrate. (b) The differential charge density maps of benzene molecules adsorbed on the Ba_2N substrate after applying electric fields of varying intensities along the z-axis direction. The isosurface value is uniformly set to 0.0015 e/Å, where the yellow regions represent charge accumulation, and the blue regions correspond to charge depletion. (c)The variation of charge transfer and equilibrium distance with the magnitude of the applied electric field, in which the blue curve denotes charge transfer and the yellow curve represents the equilibrium distance.